

---

# SR-Prominence: A Crowdsourced Protocol and Dataset Suite for Perceptually-Weighted Super-Resolution Artifact Evaluation

---

**Ivan Molodetskikh\***

AI Center, Lomonosov Moscow State University  
GSP-1, Leninskie Gory, Moscow, 119991, Russia

**Kirill Malyshev**

Lomonosov Moscow State University

**Mark Mirgaleev**

Lomonosov Moscow State University

**Evgeney Bogatyrev**

Lomonosov Moscow State University

**Nikita Zagainov**

Innopolis University  
Universitetskaya St, 1, Innopolis, Respublika Tatarstan, 420500, Russia

**Dmitriy Vatolin**

AI Center, Lomonosov Moscow State University

## Abstract

Modern image super-resolution methods generate detailed, visually appealing results, but they often introduce visual artifacts: unnatural patterns and texture distortions that degrade perceived quality. These defects vary widely in perceptual impact—some are barely noticeable, while others are highly disturbing—yet existing detection methods treat them equally. We propose artifact *prominence* as an evaluative target, defined as the fraction of viewers who judge a highlighted region to contain a noticeable artifact. We design a crowdsourced annotation protocol and construct **SR-Prominence**, a dataset suite containing 3,935 artifact masks from DeSRA, Open Images, Urban100, and a realistic no-ground-truth Urban100-HR setting, annotated with prominence. Re-annotating DeSRA reveals that 48.2% of its in-lab binary artifacts are not noticed by a majority of viewers. Across the suite, we audit SR artifact detectors, image-quality metrics, and SR methods. We find that classical full-reference metrics, especially SSIM and DISTS, provide surprisingly strong localized prominence signals, whereas no-reference IQA methods and specialized artifact detectors often fail to generalize across datasets and reference settings. SR-Prominence is released with an objective scoring protocol that allows new metrics to be benchmarked on our suite without further crowdsourcing. Together, the data and protocols enable SR artifact evaluation to move from binary defect presence toward perceptual impact. SR-Prominence is available at <https://huggingface.co/datasets/imolodetskikh/sr-artifact-prominence>.

---

\*Corresponding author: [ivan.molodetskikh@graphics.cs.msu.ru](mailto:ivan.molodetskikh@graphics.cs.msu.ru)

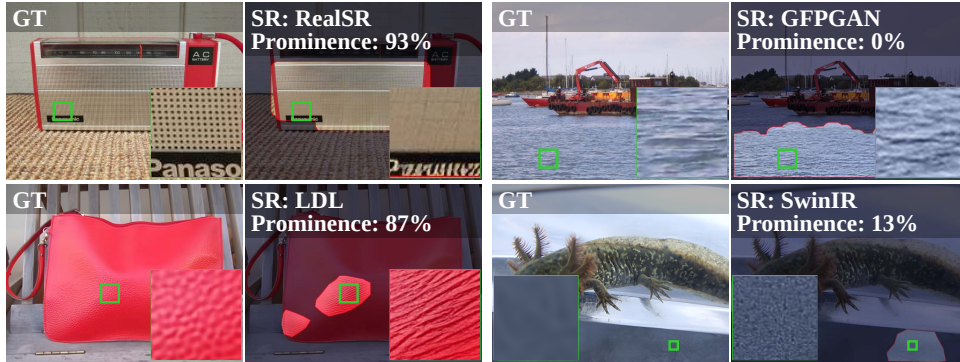


Figure 1: SR-Prominence artifact examples. Rows show Open Images (top) and DeSRA (bottom) subsets. Left: prominent artifacts; RealSR blurred out holes on the radio panel, and LDL reconstructed an incorrect linear pattern on the bag. Right: non-prominent artifacts; GFPGAN incorrectly restored a natural water surface, and SwinIR generated a dotted texture artifact on a non-salient floor region.

## 1 Introduction

Single-image super-resolution (SISR) aims to reconstruct high-resolution (HR) images from low-resolution (LR) inputs. While modern SR methods have greatly improved perceptual quality, they introduce a critical challenge: visually unpleasant artifacts. These artifacts—usually unnatural patterns, smeared faces, and texture distortions—degrade perceived quality and hinder adoption. Even the latest, most capable methods [1, 2] remain prone to generating artifacts.

Despite SISR’s growing popularity, research on detecting SR artifacts remains scarce. LDL [3] and DeSRA [4] identify artifact-prone regions using residual statistics, while segmentation-style approaches such as PAL4VST [5] predict artifact masks from the output image. These masks localize artifacts, but assign the same label to barely visible texture errors and obvious structural failures.

We use artifact *prominence* for this missing perceptual variable: the fraction of viewers who judge an artifact candidate to contain a noticeable artifact. Distortions to regular structures such as buildings, or to recognizable objects such as human faces, easily draw attention and can be distressing to viewers, while artifacts on water, grass, and other organic matter can be almost unnoticeable (Figure 1). Treating these different cases as equal carries the risk of overfitting a detection method to low-impact defects while missing the ones that viewers actually notice.

To measure prominence, we design a crowdsourced annotation protocol and use it to construct **SR-Prominence**, a four-component dataset suite. SR-Prominence contains 3,935 artifact masks generated by 15 widely-used SR methods and their variants, each with crowdsourced prominence annotations. It includes 593 existing masks from the DeSRA dataset [4] and new masks on Open Images, the standard Urban100 benchmark, and the realistic high-resolution Urban100-HR setting.

Using this suite, we audit artifact detectors, metrics, and SR models. Our analysis shows that binary labels are not enough for SR artifact evaluation: 48.2% of DeSRA’s in-lab binary artifacts are not noticed by a majority of viewers. We find that full-reference metrics such as SSIM and DISTS provide strong localized prominence signals, whereas no-reference IQA methods and specialized artifact detectors often fail to generalize. We also provide a scoring protocol for evaluating new methods on SR-Prominence without further crowdsourcing, a lightweight reference baseline, and a pseudo-GT procedure for applying full-reference metrics when high-resolution ground truth is unavailable.

Our main contributions are the following:

1. We introduce artifact *prominence* as a graded target for SR artifact evaluation and design a crowdsourced annotation protocol for collecting prominence labels. The protocol includes mask preprocessing for visual assessment and annotation quality control; we analyze response variability to justify the number of assessors.
2. We construct **SR-Prominence**, a four-component dataset suite with 3,935 prominence-annotated artifact masks generated by 15 widely-used SR methods with variants. The suite

covers existing DeSRA masks, diverse natural images from Open Images, structured scenes from Urban100, and a realistic high-resolution Urban100-HR setting.

3. We use SR-Prominence to audit SR models for their proneness to generating artifacts, and artifact detection methods, including image-quality metrics. We additionally provide a scoring protocol that requires no further crowdsourcing, a pseudo-GT procedure for applying full-reference metrics without HR ground truth, and a small artifact-detection baseline.

## 2 Related work

**SR artifacts and artifact localization.** Modern SR methods improve perceptual sharpness but can introduce visual artifacts such as hallucinated structures and texture distortions, especially with adversarial losses or large generative priors [1, 2, 6, 7]. Detection and mitigation of SISR artifacts has garnered increasing attention because these artifacts reduce perceptual quality. LDL [3] predicts pixel-level artifact maps from local residual statistics. Xie et al. [4] introduced a dataset with SR artifact masks annotated in-lab and proposed DeSRA, which contrasts GAN-SR and MSE-SR outputs to identify and suppress artifact-prone regions.

A complementary line of work treats artifact detection as segmentation, training networks on datasets with pixel-level defect maps. Given only an input image, these models predict an artifact mask. Approaches such as PAL4Inpaint [8] and PAL4VST [5] show strong generalization across generative vision tasks by localizing perceptual artifacts. Concurrently, Ren et al. [9] propose Hallucination Score that uses a multimodal LLM to provide an image-level hallucination rating for SR outputs, showing strong alignment with human judgments. The main drawback of this approach is that it lacks spatial localization, which is critical for downstream tasks such as artifact mitigation, SR model fine-tuning, and for handling cases where different regions of an image exhibit different types of artifacts.

Prior SR-artifact work therefore either provides localized but binary masks, or viewer-aligned scores without localized masks. Our work targets the missing combination: localized SR artifact candidates with graded viewer noticeability.

**Perceptual image-quality evaluation and human protocols.** SISR evaluation has traditionally relied on full-reference metrics such as PSNR and SSIM [10], which assess reconstruction fidelity but correlate poorly with perceptual quality—especially for GAN-based outputs where details and artifacts are entangled. No-reference and perceptual metrics such as LPIPS [11] and DISTS [12] better align with human perception and are now widely adopted in SR benchmarks. Some techniques aim to make metrics more artifact-resistant: ERQA [13] evaluates detail restoration by matching edges in reference and test images. However, in practice existing metrics still fall well short of matching human perception [14].

Human-judgment datasets and protocols, including PIPAL [15], LPIPS/BAPPS [11], KonIQ-10k [16], and RichHF [17], show the importance of collecting perceptual labels directly from viewers. These datasets primarily target global image quality, pairwise perceptual similarity, or generative-image feedback rather than SR artifacts. SR-Prominence applies the same general principle—human perception should define the evaluation target—to localized artifact mask candidates.

## 3 Prominence: definition and annotation protocol

Existing datasets such as DeSRA [4] contain only binary artifact masks, without information on how noticeable the artifacts are to viewers. Two masks with similar size can differ sharply in perceptual impact: distorted text or a window grid may be obvious, unlike comparable errors on plants and water. We use artifact *prominence* for this missing perceptual variable: the fraction of viewers who identify the selected region as containing a noticeable SR artifact. Each artifact sample in our datasets has a binary mask and a corresponding prominence value obtained via crowdsourced annotation.

### 3.1 Crowdsourced annotation setup

We used Yandex.Tasks to crowdsource the data collection. Participants view pairs of images labeled “Original” and “Upscaled,” with the artifact region visually highlighted. We ask them whether the highlighted region contains a distorted object or texture. Figure 2 shows an example question.

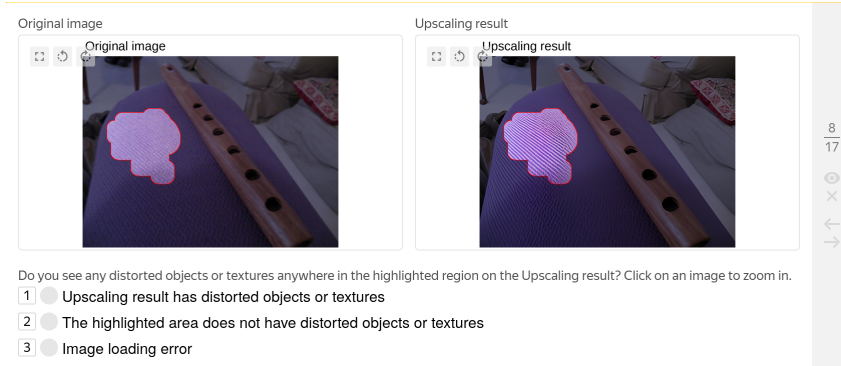


Figure 2: Viewer interface for subjective data collection.

Every image is assessed by 30 different participants. We compute prominence as the proportion of votes indicating the artifact is present. Before receiving access to the main questions, participants must answer four training questions, for which the correct answers are explained, followed by four test questions with hidden correct answers. Afterward, to ensure integrity, every group of 20 questions contains 4 random control questions. All responses from participants who make mistakes in two or more control questions within an assignment are discarded.

We selected the assessor count using a bootstrap dispersion analysis on 11 images annotated by 250 participants each; details are in Section A. Few assessors produce unstable prominence estimates; 100 assessors reduce the confidence interval to about  $\pm 10\%$ . We chose 30 assessors as a practical compromise, giving about  $\pm 20\%$  variability at substantially lower cost.

### 3.2 Choice of the “Original” image

In practical SR applications, a full-resolution reference image is unavailable: only the low-resolution input and the SR result are given. Therefore, assessment cannot rely on exact agreement with an HR ground truth, but should instead focus on the plausibility of restored details and the absence of artifacts. For the same low-resolution input, many high-resolution outputs may be acceptable. This is reflected empirically in the mismatch between rankings in SR benchmarks focused on reconstructing the original image and benchmarks focused on perceptual output quality [13, 14].

For this reason, our annotation interface uses the low-resolution input, not the high-resolution reference, as the “Original” image. In our protocol, the low-resolution image is upscaled to the target size with nearest-neighbor interpolation before being shown to participants. Nearest-neighbor interpolation makes it obvious to assessors that they are viewing the low-resolution input.

### 3.3 Mask preprocessing

An artifact-detection method should output a tight mask around an artifact, since such masks are more useful for subsequent analysis and downstream tasks such as automatic correction. However, tight masks make it harder to visually judge whether the masked area contains an artifact. Additionally, the raw output from some methods is sparse, making it extra challenging to highlight. To make masks more suitable for human viewing, we apply morphological operations before showing them to participants:

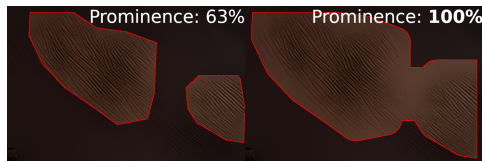


Figure 3: Example of mask preprocessing for human visual assessment.

1. Open with a  $25 \times 25$  square kernel to remove small dots in the mask.
2. Dilate with a  $64 \times 64$  circular kernel so the mask includes context around an artifact.
3. Close with a  $25 \times 25$  square kernel to eliminate holes and step away from the image borders.

The example in Figure 3 shows how a tight mask can make an artifact harder to assess compared with our preprocessing result. In Section C we verify that the effect on already-good masks is negligible.

Table 1: Overview of the SR-Prominence dataset suite.

Dataset	Source images	SR variants	Artifact masks	Total workers	Valid workers	Mean prominence	Prominent masks
Prominence-DeSRA	528	3	593	276	176	49.0%	307 (51.8%)
Prominence-OpenImages	547	15	1523	261	183	37.1%	535 (35.1%)
Prominence-Urban100	68	19	873	191	110	35.5%	241 (27.6%)
Prominence-Urban100-HR	94	16	946	164	94	24.7%	177 (18.7%)
Combined	1237	19	3935	662	425	35.6%	1260 (32.0%)

### 3.4 Cropping for large images

For Prominence-Urban100-HR we run 4× SR directly on the original Urban100 images, so the results extend beyond 4000 pixels wide and 2500 pixels tall. Our crowdsourcing platform statistics show that most participants use 1920×1080 screens. Images in full resolution would therefore be downsampled by the browser and viewed at inconsistent zoom. To remedy this, for Urban100-HR, we crop each image to a padded bounding box around the artifact-mask region before display. For the majority of the samples, this cropping procedure makes the highlighted region visible at the native scale.

## 4 SR-Prominence dataset suite

We apply the protocol described above to annotate a dataset suite of four complementary components. Each dataset component contains low-resolution input images, high-resolution SR upscaling results, binary artifact masks, and crowdsourced prominence values for every artifact mask. Together the suite contains 3,935 masks from 15 widely-used SR methods. The Urban100 components additionally evaluate two real-time SR models (SPAN and RLFN) that serve as pseudo-GT references in Section 5.3, plus a SUPIR half-precision variant and the full SeeSR model. The dataset is publicly available at <https://huggingface.co/datasets/imolodetskikh/sr-artifact-prominence>.

Table 1 summarizes the components. The worker columns report unique crowd workers who participated and who remained after quality-control filtering; in the combined row, workers shared across components are counted once. The final column reports masks with prominence  $\geq 50\%$ , i.e. at least half of valid workers confirmed the presence of an artifact.

Together, these components separate four evaluation questions: whether existing binary artifact datasets are viewer-noticeable, how SRs and detectors behave on diverse natural images, how they handle structured urban content, and how the results change in a realistic high-resolution setting.

### 4.1 Candidate-mask collection for scalable annotation

After obtaining the Prominence-DeSRA results, it became clear that a more extensive artifact dataset is necessary, covering more image content types and a wide selection of contemporary SR methods. The other three parts of our dataset suite use an automatic mask collection procedure that we designed to be able to scale to many source images and SR models. Given SR upscaling results and reference images, we run existing artifact detection and image-quality assessment methods to obtain heatmaps. The heatmaps are thresholded with fixed DeSRA-calibrated thresholds described in Section 5.1, producing candidate artifact masks. We measure the mean heatmap value inside each mask and pick the 10 strongest artifacts per metric per SR. The masks are then preprocessed following Section 3.3 and proceed to crowdsource annotation.

This fully automatic procedure scales to a large number of source images and SR methods. No expensive manual human mask drawing is required, and manual selection bias is reduced.

### 4.2 Prominence-DeSRA

For Prominence-DeSRA, we collected prominence annotations for all 593 artifact masks from the DeSRA [4] dataset. It lets us directly test whether binary in-lab artifact masks correspond to viewer-noticeable artifacts, but it is not sufficient as a general prominence benchmark. It covers only three SR methods and does not test modern diffusion- or transformer-based SR systems across diverse image content. We therefore extend the suite along three axes that are important for prominence-aware SR

evaluation: broader natural-image diversity, structured scenes where localized artifacts are especially visible, and a deployment-style setting without HR ground truth.

### 4.3 Prominence-OpenImages

Prominence-OpenImages targets diverse natural-image SR artifacts. We randomly selected 2,101 source photos from Open Images [18], each at 1024×768 pixels, downsampled them by 4× with bicubic interpolation, and upsampled them with 15 popular SR methods and variants.

The first 697 masks came from manual annotation and from existing visual-quality metrics or artifact detectors, including SSIM, DISTS, LPIPS, LDL, and DeSRA. Afterward, we used our fully-automatic mask proposal pipeline with no manual curation to collect the remaining 826 masks. Of the 2,101 source photos, 547 contributed at least one selected mask and form the Prominence-OpenImages source set reported in Table 1. The summary Tables 3 and 5 report SR and metric results only on the uncurated subset to avoid bias.

### 4.4 Prominence-Urban100

Prominence-OpenImages provides broad natural-image coverage, but many prominent SR artifacts occur in structured content such as text, façades, window grids, signs, and repeated patterns. Prominence-Urban100 targets this setting using a standard SR benchmark whose regular structures are known to stress SR methods. It lets the suite test whether prominence depends on semantic and geometric context rather than only on generic image diversity. This component is based on the standard Urban100 SR test set [19]. It contains 873 masks from 68 source images and 19 SR settings, collected with the fully uncurated procedure.

### 4.5 Prominence-Urban100-HR

Prominence-Urban100-HR is a more challenging and realistic variant of Prominence-Urban100. Instead of the downsample-then-upsample setting, we took the original high-resolution Urban100 images and upsampled them as-is, with no additional processing or synthetic degradation. This part of the dataset contains 946 masks from 94 source images and 16 SR settings (fewer, as the VRAM constraints allowed). Its mean prominence is lower than the other dataset components, which is expected as the 4× larger source images make details clearer and easier to upscale.

No higher-resolution ground truth exists for these outputs, reducing SR-overfitting risk. The human annotations do not require such a reference, since workers compare the SR output to the LR-derived original as in Section 3. For full-reference metric evaluation only, we use the RLFN pseudo-GT protocol described in Section 5.3.

## 5 Benchmark tasks and scoring

We will now define SR-Prominence benchmark tasks, scoring, and reference protocols.

### 5.1 Uncurated top-artifact benchmark

The uncurated benchmark evaluates whether SR models and detection methods expose artifacts that viewers actually notice. For each dataset component, we report two complementary views. Detector tables group masks by the metric that found them and measure whether that metric finds prominent artifacts. SR tables group masks by the SR model that produced the output and measure whether an SR model tends to produce prominent artifacts. For detector tables, higher mean prominence and more confident masks are better. For SR tables, lower values are better.

This evaluation required thresholding raw metric output to get candidate masks as described in Section 4.1. Following [4], we selected the thresholds for each method by maximizing the Precision × Recall product on the prominent subset of the DeSRA dataset (307 masks).

For per-SR tables, when multiple metrics found an artifact mask on the same SR image, we deduplicated these masks by selecting the one with the highest prominence value. This way, SR outputs containing prominent artifacts are not overcounted in the scores.

Table 2: Crowd-sourced prominence results across SR models (DeSRA).

SR	Family	Masks	Mean Prominence <sup>↓</sup>	Conf. Masks <sup>↓</sup>
SwinIR [20]	Transformer	206	<b>42.15%</b>	<b>78</b>
RealESRGAN [7]	CNN	199	46.52%	97
LDL-SR [3]	CNN	188	59.28%	132

## 5.2 Threshold-free scoring approach

The uncurated benchmark above evaluates thresholded candidate masks that were shown to crowd workers. It is the primary benchmark because the final target is viewer prominence. However, it is expensive to extend to every new SR or detection method, since each additional mask requires crowdsourced annotations. We therefore propose a threshold-free objective score that measures how well an artifact detection method evaluates artifact prominence on our dataset suite.

A detection method is run on all input images from the dataset, producing spatial heatmaps for each of them. For each annotated mask, we compute the median heatmap value inside the mask and subtract the median heatmap value outside the mask. Subtracting the outside value makes the score less sensitive to cross-image and cross-SR variation. For masks that were dilated during the visual-assessment preprocessing in Section 3.3, we first erode them back, so that the inside region better matches the original artifact localization.

We then compute Spearman correlation between this contrast value and the crowdsourced prominence over all masks in a dataset component:  $SRCC(\text{inside}_{p50} - \text{outside}_{p50}, \text{GT prominence})$ . A high positive correlation means that the detector not only responds inside the annotated regions, but responds more strongly for artifacts noticed by more viewers. For binary detectors, we apply the same calculation to their binary masks.

This score is designed for rapid benchmarking after the prominence annotations have been collected. It cannot reveal artifacts that no detector proposed. Instead, it provides a way to compare heatmaps and reference choices without additional crowdsourcing. Table 4 shows this score for the evaluated methods. For verification, we compared scores with the Prom.  $\times$  Conf. crowdsourced rankings on Open Images, Urban100, and Urban100-HR, obtaining Spearman correlations 0.886, 0.750, 0.786.

## 5.3 Adapting full-reference metrics to no-HR settings with pseudo-GT

Full-reference metrics provide more-accurate detail restoration quality scores for SR by using pixel-level information from the reference image. The use of such metrics in SR creates difficulties, however, since the SR-output resolution is higher than that of the original low-resolution frame. This restriction is unavoidable for Prominence-Urban100-HR, which has no high-resolution ground truth.

To employ full-reference metrics in this setting, we use the following pipeline. We apply a lightweight SR method to the original low-resolution frame, thereby obtaining a pseudo-GT, and then calculate the metric between this pseudo-GT and the SR output. The pseudo-GT model should be conservative: it may trail heavier SR models in visual quality, but it should avoid producing prominent artifacts of its own. Real-time SR methods such as SPAN [21] and RLFN [22] are natural candidates for this role. In our experiments we use RLFN, which is less artifact-prone than SPAN on Urban100 in Table 5.

When serving as pseudo-GT for full-reference metrics, the artifact-detection performance drop is small compared with using the original HR frames. We characterize this approximation in Table 4.

## 5.4 Baseline artifact detection method

To accompany the dataset and evaluation protocol, we provide a simple reference baseline that predicts a spatial artifact-prominence heatmap for a super-resolved image. The baseline computes three complementary heatmaps: block-wise DISTs, which is strong in our metric analysis, and two features adapted from JPEG AI artifact work [23]: *ssm\_jup*, an RGB adaptation of a local residual-variance detector, and *bd\_jup*, a block-wise combination of LPIPS and ERQA. A shallow MLP fuses these features independently at each pixel and is trained on 374 Prominence-OpenImages artifact examples to match the crowdsourced prominence inside the annotated mask and zero outside it. Despite this limited training setup, the baseline generalizes to held-out OpenImages examples and

Table 3: Crowd-sourced prominence results across artifact detection methods.

Method	Open Images				Urban100				Urban100-HR				Avg. Rank <sup>↓</sup>
	Masks Found	Mean Prominence <sup>↑</sup>	Conf. Masks Found <sup>†</sup>	Prom. × Conf. <sup>†</sup>	Masks Found	Mean Prominence <sup>†</sup>	Conf. Masks Found <sup>†</sup>	Prom. × Conf. <sup>†</sup>	Masks Found	Mean Prominence <sup>†</sup>	Conf. Masks Found <sup>†</sup>	Prom. × Conf. <sup>†</sup>	
bd_jup (t=0.1)	150	22.20%	27	5.99%	190	32.28%	37	11.94%	160	12.58%	6	0.75%	6.3
LDL (t=0.005)	23	<b>70.23%</b>	17	11.94%	1	6.67%	0	0.00%	113	24.32%	15	3.65%	5.7
ssm_jup (t=0.15)	150	26.91%	36	9.69%	155	34.03%	41	13.95%	160	11.44%	8	0.92%	5.3
DeSRA	120	34.72%	38	13.19%	10	<b>56.83%</b>	6	3.41%	39	<b>48.35%</b>	20	9.67%	4.3
Baseline (t=0.3)	139	43.07%	55	<b>23.69%</b>	140	39.29%	46	18.07%	160	27.59%	32	8.83%	2.3
DISTS (t=0.25)	148	41.31%	57	23.55%	190	34.28%	47	16.11%	160	32.40%	46	<b>14.90%</b>	<b>2.0</b>
SSIM (t=0.55)	114	41.73%	47	19.61%	187	37.02%	58	<b>21.47%</b>	154	32.77%	41	13.44%	<b>2.0</b>

Table 4: Threshold-free prominence score described in Section 5.2. RLFN columns use the pseudo-GT protocol from Section 5.3.

Reference Input	Open Images		Urban100		Urban100-HR	DeSRA		Avg. Rank <sup>↓</sup>
	Original HR	RLFN	Original HR	RLFN	RLFN	MSE-SR	RLFN	Rank <sup>↓</sup>
TOPIQ (no-ref)	-0.096	-0.096	-0.099	-0.099	-0.015	-0.114	-0.114	11.9
PaQ-2-PiQ (no-ref)	-0.097	-0.097	-0.222	-0.222	0.024	-0.088	-0.088	11.7
ERQA	0.142	-0.134	0.197	0.138	0.025	-0.024	0.023	8.7
PAL4VST (bin., no-ref)	0.136	0.136	0.145	0.145	N/A	0.043	0.043	7.7
PAL4Inpaint (bin., no-ref)	0.067	0.067	0.156	0.156	0.112	0.109	0.109	7.4
DeSRA	0.303	0.299	0.019	0.049	0.340	0.021	-0.003	7.3
bd_jup	0.346	0.177	0.236	0.245	0.267	-0.105	-0.098	6.6
LIPS	0.446	0.304	0.213	0.234	<b>0.446</b>	-0.138	-0.132	6.0
ssm_jup	0.321	0.237	0.092	0.099	0.099	<b>0.342</b>	<b>0.331</b>	6.0
LDL	0.288	0.233	0.158	0.200	0.255	0.193	0.177	5.9
SSIM	0.312	0.297	<b>0.305</b>	0.264	0.348	-0.010	-0.020	4.9
DISTS	0.415	0.370	0.236	<b>0.283</b>	0.401	-0.039	-0.009	4.1
Baseline	<b>0.555</b>	<b>0.374</b>	0.256	0.241	0.394	0.213	0.212	<b>2.1</b>

to the Urban100, Urban100-HR, and DeSRA components, achieving the best average rank in the threshold-free prominence score in Table 4.

## 6 Empirical findings from prominence-aware evaluation

We use SR-Prominence to audit binary masks, detectors, image-quality metrics, and SR models.

### 6.1 Binary masks are insufficient annotation for SR artifacts

Table 2 shows per-SR prominence results that we obtained on the DeSRA dataset. This dataset provides artifact masks for three SR methods annotated in-lab, so it was surprising to learn that only in 307 of 593 masks at least half of workers confirmed the artifact under our protocol. Equivalently, 48.2% of DeSRA binary artifacts are not noticed by a majority of crowd workers. This result is the cleanest evidence in our suite that binary artifact masks are insufficient for SR artifact assessment.

### 6.2 Full-reference metrics provide better prominence signals than no-reference ones

Table 3 shows the results of the uncurated crowdsourced detector benchmark.

LDL with a 0.005 threshold finds highly visible artifacts on Open Images, but it trails far behind other methods in total number of confident masks. To account for both of these scores, we multiplied them; the results are in the “Prom. × Conf.” column. This combined score rewards detectors that find many prominent artifacts rather than only a few high-prominence examples. We tested LDL at two lower thresholds, which increased the total masks found, but they mainly captured non-prominent artifacts, yielding even worse combined score. This follows the same intuition as the Precision × Recall threshold criterion used by [4]: both coverage and confidence matter.

Across the three uncurated dataset components, DISTS and SSIM are the strongest existing metrics by average rank, showing better performance than DeSRA and LDL—purpose-made SR artifact detectors. This is notable as neither metric was designed for SR-artifact assessment, especially so SSIM, a classical image-quality assessment metric. DISTS is a learned perceptual similarity metric trained on natural images to account for texture distortions, which makes its strong performance less surprising. Together, these results show that full-reference structural and perceptual similarity metrics contain the most useful information about viewer-noticeable SR failures.

Table 5: Crowd-sourced prominence results across SR models.

SR	Family	Open Images			Urban100			Urban100-HR		
		Masks Found	Mean Prominence <sup>↓</sup>	Conf. Masks Found <sup>↓</sup>	Masks Found	Mean Prominence <sup>↓</sup>	Conf. Masks Found <sup>↓</sup>	Masks Found	Mean Prominence <sup>↓</sup>	Conf. Masks Found <sup>↓</sup>
LDL-SR [3]	CNN	52	66.19%	19	52	54.66%	17	60	39.20%	9
RealESRGAN [7]	CNN	61	48.42%	19	51	47.01%	12	55	31.71%	11
SwinIR [20]	Transformer	59	41.09%	17	51	39.49%	10	61	33.54%	12
GFPGAN [24]	CNN	45	32.74%	11	54	52.17%	14	56	39.94%	12
SUPIR [1]	Diffusion	70	45.29%	20	50	26.90%	4	-	-	-
StableSR [2]	Diffusion	50	33.18%	13	50	35.39%	7	62	26.81%	11
OSDiff [25]	Diffusion	50	30.33%	12	50	42.24%	11	55	22.92%	7
RealSR [26]	CNN	51	28.70%	10	47	48.22%	14	67	27.19%	5
PASD-SDXL [27]	Diffusion	69	35.95%	12	51	27.77%	6	70	29.22%	10
SecSR-turbo [28]	Diffusion	61	32.34%	14	50	26.82%	4	66	25.47%	9
SinSR [29]	Diffusion	60	19.39%	3	46	43.87%	11	55	28.26%	5
SPAN [21]	CNN	-	-	-	36	43.97%	9	48	21.47%	3
StableSR-turbo [2]	Diffusion	60	28.55%	14	50	24.33%	2	56	17.01%	3
RLFN [22]	CNN	-	-	-	36	31.10%	4	-	-	-
SUPIR-half [1]	Diffusion	-	-	-	50	26.08%	4	-	-	-
ResShift [30]	Diffusion	60	20.22%	7	42	36.99%	6	59	21.05%	4
SeeSR [28]	Diffusion	-	-	-	50	26.57%	4	61	23.42%	4
HAT-L [31]	Transformer	53	13.53%	1	29	22.80%	1	60	15.48%	1
DRCT [32]	Transformer	43	11.85%	1	28	21.47%	0	55	12.38%	1

The threshold-free analysis in Table 4 supports the same conclusion from a different viewpoint, and includes a wider selection of metrics. No-reference methods are generally worse than the methods that can use an HR or pseudo-GT reference, with no-reference IQA methods in particular having correlations close to zero or negative on several components. This is expected for whole-image no-reference IQA metrics, which are hard to adapt to localized prominence evaluation because their original target is global image quality. The same limitation appears for no-reference artifact detectors PAL4Inpaint and PAL4VST: despite being designed to localize perceptual artifacts, and despite PAL4VST including SR among its target distortion sets, they rank prominence poorly.

### 6.3 Artifact-aware SR training does not guarantee low-prominence artifacts

Table 5 shows the uncurated crowdsourced benchmark results grouped by the SR model that produced each candidate artifact mask. Surprisingly, LDL-SR is the weakest method across all three components, with the highest mean prominence and many confident masks on both Open Images and Urban100, despite being specifically trained for artifact prevention. This is consistent with the Prominence-DeSRA result in Table 2, where LDL-SR also produces the most prominent artifacts.

The most robust methods in our benchmark are DRCT and HAT-L. They have the lowest mean prominence on every reported component and produce at most one confident mask in each setting, with DRCT producing none on Urban100. This suggests that strong reconstruction-oriented Transformer SR can avoid prominent artifacts more reliably than generative methods.

The Urban100 and Urban100-HR results separate two difficult structured-scene settings. In the standard downsample-then-upsample setting, several methods show much higher prominence on Urban100 than on Urban100-HR, with OSDiff, RealSR, SinSR, and SPAN dropping by 15–22%. This suggests that the synthetic benchmark setting can amplify visible failures on structured content. At the same time, the no-HR Urban100-HR setting is not merely easier: LDL-SR, GFPGAN, and SwinIR still produce many prominent masks, while HAT-L and DRCT remain robust. The two Urban100 components therefore probe distinct failure modes, not just varying difficulty.

### 6.4 Artifact type and semantic context matter

To characterize where prominent SR artifacts occur, we additionally annotated artifact types and semantic context with Qwen 3 VLM (Section D). Among the most prominent types are hallucinated texture and text aberrations, with plastic texture being less noticeable. By semantic context, artifacts in art and text images are the most prominent, while artifacts in nature images are the least. These results support the design of SR-Prominence: it combines broad natural-image diversity with urban scenes, covering contexts in which the same nominal artifacts can have different perceptual impact.

## 7 Limitations and future work

The main limitation of SR-Prominence is the lack of precise artifact masks, as delineating exact artifact boundaries is ambiguous even for human annotators. Instead, we seed masks using existing methods, introducing some inaccuracy. Consequently, models trained on this data may have lower performance due to imperfect supervision. Our pseudo-GT procedure is also only an approximation. It allows full-reference metrics to be applied in a realistic no-HR setting, but can produce false positives when the lightweight SR model used as pseudo-GT fails to reconstruct fine textures.

Future work could extend prominence modeling to video super-resolution. We consider images independently and do not address temporal artifacts such as flickering. Another direction is semantic artifacts: higher-capacity models such as SUPIR move from simple texture distortions toward more semantic failures like object replacement, which may need adjustments to annotation and evaluation.

## 8 Conclusion

We introduced artifact prominence as a viewer-centered target for super-resolution artifact evaluation and constructed SR-Prominence, a four-component dataset suite of prominence-annotated artifact masks. Instead of treating all localized defects as equal, prominence measures how often viewers judge a region to contain a noticeable artifact. Our results show that binary artifact labels are insufficient: roughly half of DeSRA binary masks are not noticed by a majority of crowd workers.

Across the broader suite, full-reference metrics provide strong localized prominence signals, while no-reference IQA methods and specialized artifact detectors often fail to generalize. The SR-model audit further shows that artifact-aware training does not necessarily reduce prominent artifacts.

SR-Prominence is intended to make SR artifact evaluation more perceptually grounded. The released annotations, scoring protocol, pseudo-GT procedure, and reference baseline allow future detectors and SR methods to be evaluated against viewer noticeability without repeating the full crowdsourcing process. More broadly, our findings suggest that SR artifact evaluation should move beyond binary defect presence and account for which artifacts viewers actually notice.

## Acknowledgments

The research was carried out using the MSU-270 supercomputer of Lomonosov Moscow State University.

We’d like to thank Valeriy Gorbachev for conducting the VLM annotation for Section 6.4.

## References

- [1] F. Yu, J. Gu, Z. Li, J. Hu, X. Kong, X. Wang, J. He, Y. Qiao, and C. Dong, “Scaling up to excellence: Practicing model scaling for photo-realistic image restoration in the wild,” in *Proceedings of the IEEE/CVF Conference on Computer Vision and Pattern Recognition (CVPR)*, pp. 25669–25680, June 2024.
- [2] J. Wang, Z. Yue, S. Zhou, K. C. Chan, and C. C. Loy, “Exploiting diffusion prior for real-world image super-resolution,” *International Journal of Computer Vision*, 2024.
- [3] J. Liang, H. Zeng, and L. Zhang, “Details or artifacts: A locally discriminative learning approach to realistic image super-resolution,” in *Proceedings of the IEEE/CVF Conference on Computer Vision and Pattern Recognition*, pp. 5657–5666, 2022.
- [4] L. Xie, X. Wang, X. Chen, G. Li, Y. Shan, J. Zhou, and C. Dong, “DeSRA: detect and delete the artifacts of gan-based real-world super-resolution models,” *arXiv preprint arXiv:2307.02457*, 2023.
- [5] L. Zhang, Z. Xu, C. Barnes, Y. Zhou, Q. Liu, H. Zhang, S. Amirghodsi, Z. Lin, E. Shechtman, and J. Shi, “Perceptual artifacts localization for image synthesis tasks,” in *Proceedings of the IEEE/CVF International Conference on Computer Vision (ICCV)*, pp. 7579–7590, October 2023.

- [6] C. Ledig, L. Theis, F. Huszár, J. Caballero, A. Cunningham, A. Acosta, A. Aitken, A. Tejani, J. Totz, Z. Wang, *et al.*, “Photo-realistic single image super-resolution using a generative adversarial network,” in *Proceedings of the IEEE conference on computer vision and pattern recognition*, pp. 4681–4690, 2017.
- [7] X. Wang, L. Xie, C. Dong, and Y. Shan, “Real-ESRGAN: Training real-world blind super-resolution with pure synthetic data,” in *Proceedings of the IEEE/CVF international conference on computer vision*, pp. 1905–1914, 2021.
- [8] L. Zhang, Y. Zhou, C. Barnes, S. Amirghodsi, Z. Lin, E. Shechtman, and J. Shi, “Perceptual artifacts localization for inpainting,” *arXiv preprint arXiv:2208.03357*, 2022.
- [9] W. Ren, R. Goyal, Z. Hu, T. T. Aumentado-Armstrong, I. Mohamed, and A. Levinshtein, “Hallucination score: Towards mitigating hallucinations in generative image super-resolution,” 2025.
- [10] Z. Wang, A. C. Bovik, H. R. Sheikh, and E. P. Simoncelli, “Image quality assessment: from error visibility to structural similarity,” *IEEE transactions on image processing*, vol. 13, no. 4, pp. 600–612, 2004.
- [11] R. Zhang, P. Isola, A. A. Efros, E. Shechtman, and O. Wang, “The unreasonable effectiveness of deep features as a perceptual metric,” in *Proceedings of the IEEE conference on computer vision and pattern recognition*, pp. 586–595, 2018.
- [12] K. Ding, K. Ma, S. Wang, and E. P. Simoncelli, “Image quality assessment: Unifying structure and texture similarity,” *IEEE Transactions on Pattern Analysis and Machine Intelligence*, vol. 44, no. 5, pp. 2567–2581, 2022.
- [13] A. Kirillova, E. Lyapustin, A. Antsiferova, and D. Vatolin, “ERQA: Edge-restoration quality assessment for video super-resolution,” in *Proceedings of the 17th International Joint Conference on Computer Vision, Imaging and Computer Graphics Theory and Applications - Volume 4: VISAPP*, pp. 315–322, INSTICC, SciTePress, 2022.
- [14] A. Borisov, E. Bogatyrev, and D. Vatolin, “MSU video super-resolution quality metrics benchmark.” <https://videoprocessing.ai/benchmarks/super-resolution-metrics.html>, 2025. Accessed: 2026-01-28.
- [15] G. Jinjin, C. Haoming, C. Haoyu, Y. Xiaoxing, J. S. Ren, and D. Chao, “PIPAL: A large-scale image quality assessment dataset for perceptual image restoration,” in *European Conference on Computer Vision*, pp. 633–651, 2020.
- [16] V. Hosu, H. Lin, T. Sziranyi, and D. Saupe, “KonIQ-10k: An ecologically valid database for deep learning of blind image quality assessment,” *IEEE Transactions on Image Processing*, vol. 29, pp. 4041–4056, 2020.
- [17] Y. Liang, J. He, G. Li, P. Li, A. Klimovskiy, N. Carolan, J. Sun, J. Pont-Tuset, S. Young, F. Yang, *et al.*, “Rich human feedback for text-to-image generation,” in *Proceedings of the IEEE/CVF Conference on Computer Vision and Pattern Recognition*, pp. 19401–19411, 2024.
- [18] A. Kuznetsova, H. Rom, N. Alldrin, J. Uijlings, I. Krasin, J. Pont-Tuset, S. Kamali, S. Popov, M. Mallocci, A. Kolesnikov, *et al.*, “The open images dataset v4: Unified image classification, object detection, and visual relationship detection at scale,” *International journal of computer vision*, vol. 128, no. 7, pp. 1956–1981, 2020.
- [19] J.-B. Huang, A. Singh, and N. Ahuja, “Single image super-resolution from transformed self-exemplars,” in *Proceedings of the IEEE Conference on Computer Vision and Pattern Recognition (CVPR)*, June 2015.
- [20] J. Liang, J. Cao, G. Sun, K. Zhang, L. Van Gool, and R. Timofte, “SwinIR: Image restoration using swin transformer,” in *Proceedings of the IEEE/CVF international conference on computer vision*, pp. 1833–1844, 2021.

- [21] C. Wan, H. Yu, Z. Li, Y. Chen, Y. Zou, Y. Liu, X. Yin, and K. Zuo, “Swift parameter-free attention network for efficient super-resolution,” in *Proceedings of the IEEE/CVF Conference on Computer Vision and Pattern Recognition*, pp. 6246–6256, 2024.
- [22] F. Kong, M. Li, S. Liu, D. Liu, J. He, Y. Bai, F. Chen, and L. Fu, “Residual local feature network for efficient super-resolution,” in *2022 IEEE/CVF Conference on Computer Vision and Pattern Recognition Workshops (CVPRW)*, pp. 765–775, 2022.
- [23] D. Tsereh, M. Mirgaleev, I. Molodetskikh, R. Kazantsev, and D. S. Vatolin, “JPEG AI image compression visual artifacts: Detection methods and dataset,” *ArXiv*, vol. abs/2411.06810, 2024.
- [24] X. Wang, Y. Li, H. Zhang, and Y. Shan, “Towards real-world blind face restoration with generative facial prior,” in *Proceedings of the IEEE/CVF conference on computer vision and pattern recognition*, pp. 9168–9178, 2021.
- [25] R. Wu, L. Sun, Z. Ma, and L. Zhang, “One-step effective diffusion network for real-world image super-resolution,” *Advances in Neural Information Processing Systems*, vol. 37, pp. 92529–92553, 2024.
- [26] X. Ji, Y. Cao, Y. Tai, C. Wang, J. Li, and F. Huang, “Real-world super-resolution via kernel estimation and noise injection,” in *The IEEE/CVF Conference on Computer Vision and Pattern Recognition (CVPR) Workshops*, June 2020.
- [27] T. Yang, R. Wu, P. Ren, X. Xie, and L. Zhang, “Pixel-aware stable diffusion for realistic image super-resolution and personalized stylization,” in *European conference on computer vision*, pp. 74–91, Springer, 2024.
- [28] R. Wu, T. Yang, L. Sun, Z. Zhang, S. Li, and L. Zhang, “SeeSR: Towards semantics-aware real-world image super-resolution,” in *Proceedings of the IEEE/CVF conference on computer vision and pattern recognition*, pp. 25456–25467, 2024.
- [29] Y. Wang, W. Yang, X. Chen, Y. Wang, L. Guo, L.-P. Chau, Z. Liu, Y. Qiao, A. C. Kot, and B. Wen, “SinSR: diffusion-based image super-resolution in a single step,” in *Proceedings of the IEEE/CVF Conference on Computer Vision and Pattern Recognition*, pp. 25796–25805, 2024.
- [30] Z. Yue, J. Wang, and C. C. Loy, “ResShift: Efficient diffusion model for image super-resolution by residual shifting,” *Advances in Neural Information Processing Systems*, vol. 36, pp. 13294–13307, 2023.
- [31] X. Chen, X. Wang, W. Zhang, X. Kong, Y. Qiao, J. Zhou, and C. Dong, “HAT: Hybrid attention transformer for image restoration,” *arXiv preprint arXiv:2309.05239*, 2023.
- [32] C.-C. Hsu, C.-M. Lee, and Y.-S. Chou, “DRCT: Saving image super-resolution away from information bottleneck,” in *Proceedings of the IEEE/CVF Conference on Computer Vision and Pattern Recognition (CVPR) Workshops*, pp. 6133–6142, June 2024.
- [33] D. Martin, C. Fowlkes, and J. Malik, “BSDS200 dataset.” <https://huggingface.co/datasets/goodfellowliu/BSDS200>, 2001. License: Apache 2.0.
- [34] X. Wang, K. Yu, *et al.*, “Historical dataset.” <https://github.com/xinntao/BasicSR>, 2018. Part of BasicSR library (license not explicitly specified).
- [35] C. Dong and C. C. Loy, “General-100 dataset.” <http://mmlab.ie.cuhk.edu.hk/projects/FSRCNN.html>, 2016. License: OpenRail.
- [36] M. Bevilacqua, A. Roumy, and C. Guillemot, “Set5 and set14 datasets.” [https://figshare.com/articles/dataset/BSD100\\_Set5\\_Set14\\_Urban100/21586188](https://figshare.com/articles/dataset/BSD100_Set5_Set14_Urban100/21586188), 2012. License: CC0 1.0 Universal.
- [37] J. Yang, J. Wright, and T. Huang, “T91 super-resolution dataset.” <https://github.com/open-mmlab/mmsr>, 2010. License: DbCL 1.0.

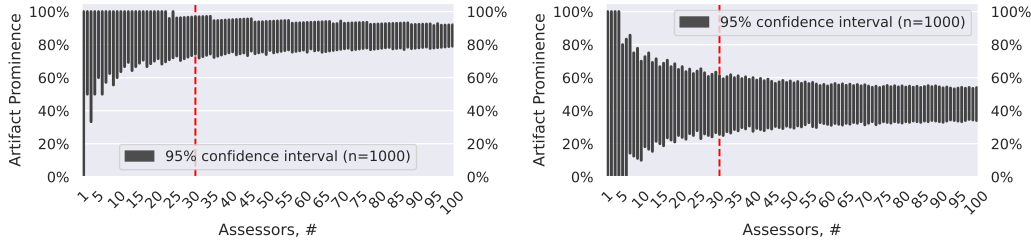


Figure 4: Bootstrap-analysis results for an image with a highly prominent artifact (left) and barely prominent artifact (right). Red line indicates our chosen assessor count of 30.

## A Crowdsourced annotation dispersion analysis

We motivate our choice to use 30 assessors for every image by analyzing answer dispersion. For this analysis, we selected 11 SR-upscaled images containing artifacts of varying intensity and conducted crowdsourced annotation following the same procedure, but with a higher participant count: every image was assessed by 250 participants instead of 30. Next, we performed a bootstrap analysis on the votes. For each assessor count  $k$  from 1 to 100, the analysis randomly sampled  $k$  votes with replacement and computed the prominence from these votes. This procedure was repeated  $n=1000$  times; we then computed 95% confidence intervals for each assessor count  $k$ .

Figure 4 shows these confidence intervals for two sample images: one with a highly prominent artifact and another with a barely prominent artifact. In cases with few assessors (1–5), the confidence interval frequently spans the whole prominence range from 0% to 100%, meaning any given 5 assessors may all state that an artifact is present or absent. This is especially true for unclear cases at around 50% prominence. By 100 assessors, the confidence interval shrinks to about  $\pm 10\%$ .

For the rest of our annotation process we chose an assessor count of 30 as a reasonable compromise between the confidence of the result ( $\pm 20\%$ ) and the time/cost of using many assessors.

## B Crowdsourcing worker instructions

The full worker instructions were as follows:

In this task, you will see images before and after upscaling. You need to look at the upscaling result and choose whether it contains distorted objects or textures.

Pay attention to the highlighted regions; they are lighter and outlined with red boxes.

**How to complete the task:** Look at the Original image to understand what is shown in the frame. Then carefully examine the highlighted region in the Upscaling Result. Choose one of the answer options.

If you see distorted objects or textures anywhere inside the highlighted region in the Upscaling Result, choose **Upscaling result has distorted objects or textures**. If you do not see distorted objects or textures in the Upscaling Result, choose **The highlighted region does not have distorted objects or textures**. If the image failed to load, choose **Image loading error**.

Please be careful, as the task includes control questions.

Click on the image to enlarge it and examine it more closely. If the image is rotated, click the Rotate button. Skip tasks where more than half of the images failed to load. On a computer, you can use the 1, 2, 3, and arrow keys.

## C Mask-preprocessing impact on DeSRA

The DeSRA dataset contains in-lab annotated masks that are not sparse and are generally suitable for human viewing as is. We used those masks to verify the impact of our preprocessing step by running the crowdsourced prominence annotation twice: once with our preprocessing and once with

Table 6: Qwen 3 VLM artifact-type labels across SR-Prominence. Each cell reports  $n$  / mean prominence / prominent rate.

Artifact type	DeSRA	OpenImages	Urban100	Urban100-Up	Total
hallucinated texture	325 / 0.580 / 68.0%	812 / 0.479 / 50.0%	701 / 0.398 / 34.0%	539 / 0.274 / 22.4%	2377 / 0.423 / 41.5%
plastic texture	364 / 0.431 / 42.3%	934 / 0.283 / 22.7%	416 / 0.323 / 23.8%	446 / 0.212 / 13.5%	2160 / 0.301 / 24.3%
text aberrations	–	146 / 0.523 / 56.8%	27 / 0.281 / 7.4%	10 / 0.263 / 30.0%	183 / 0.473 / 48.1%
face distortion	–	42 / 0.455 / 42.9%	16 / 0.424 / 25.0%	4 / 0.983 / 100.0%	62 / 0.481 / 41.9%
color change	4 / 0.425 / 50.0%	8 / 0.263 / 12.5%	10 / 0.336 / 30.0%	2 / 0.383 / 0.0%	24 / 0.330 / 25.0%
deblurring	14 / 0.233 / 14.3%	–	–	–	14 / 0.233 / 14.3%
other	–	–	–	3 / 0.078 / 0.0%	3 / 0.078 / 0.0%

Table 7: Qwen 3 VLM semantic-context labels across SR-Prominence. Each cell reports  $n$  / mean prominence / prominent rate.

Semantic context	DeSRA	OpenImages	Urban100	Urban100-Up	Total
urban	91 / 0.379 / 35.2%	455 / 0.385 / 36.3%	822 / 0.366 / 29.0%	885 / 0.245 / 18.3%	2253 / 0.323 / 26.5%
objects	390 / 0.512 / 55.1%	1043 / 0.426 / 42.8%	205 / 0.368 / 29.3%	425 / 0.222 / 15.3%	2063 / 0.394 / 38.1%
texture	94 / 0.538 / 58.5%	259 / 0.328 / 28.2%	322 / 0.313 / 20.5%	367 / 0.188 / 11.7%	1042 / 0.293 / 22.7%
people	120 / 0.483 / 48.3%	257 / 0.383 / 38.9%	197 / 0.368 / 26.9%	191 / 0.307 / 29.8%	765 / 0.376 / 35.0%
text	79 / 0.521 / 57.0%	343 / 0.458 / 48.1%	110 / 0.350 / 24.5%	68 / 0.346 / 29.4%	600 / 0.434 / 42.8%
nature	131 / 0.433 / 39.7%	370 / 0.211 / 13.2%	24 / 0.205 / 0.0%	11 / 0.121 / 9.1%	536 / 0.263 / 19.0%
animals	219 / 0.487 / 52.1%	197 / 0.277 / 20.3%	–	–	416 / 0.387 / 37.0%
action	68 / 0.474 / 50.0%	107 / 0.313 / 26.2%	39 / 0.410 / 38.5%	90 / 0.330 / 36.7%	304 / 0.366 / 36.2%
art	12 / 0.527 / 75.0%	99 / 0.400 / 39.4%	101 / 0.589 / 63.4%	22 / 0.270 / 9.1%	234 / 0.476 / 48.7%

unmodified masks. For this comparison, separate groups of participants conducted the annotations, with matching question order. The mean artifact prominence for the entire DeSRA dataset was 49.4% with our preprocessing and 47.7% with the original masks. This small difference, well within annotation noise, indicates that preprocessing does not meaningfully change the outcome for masks that are already good for visual inspection.

## D Artifact-type and semantic-context analysis

We used the Qwen 3 VLM to assign auxiliary artifact-type labels to each annotated mask and semantic-context labels to each source image. We then hand-checked and cleaned the artifact-type labels. These labels are multi-valued and model-generated, so they are intended for aggregate descriptive analysis rather than as ground-truth classes. In the following tables, prominent rate is the fraction of masks with crowdsourced prominence  $\geq 0.5$ , i.e. masks for which at least half of retained workers confirmed a noticeable artifact. Counts across rows need not sum to the dataset size because each mask or source image may receive multiple labels.

Across the labeled datasets, artifact prominence differs substantially by artifact type. Plastic texture is the least prominent common artifact type, appearing in 2160 masks with mean prominence 0.301 and 24.3% prominent masks. In contrast, hallucinated texture appears in 2377 masks with mean prominence 0.423 and 41.5% prominent masks, suggesting that viewers are more sensitive to false structured detail, moiré, or invented texture than to over-smoothed or waxy surfaces. Text aberrations are also high-prominence overall, appearing in 183 masks with mean prominence 0.473 and 48.1% prominent masks.

Semantic context shows a similar pattern. The highest-prominence source-image contexts are art, with 234 masks, mean prominence 0.476, and 48.7% prominent masks, and text, with 600 masks, mean prominence 0.434 and 42.8% prominent masks. The lowest-prominence contexts are nature, with 536 masks, mean prominence 0.263 and 19.0% prominent masks, and texture, with 1042 masks, mean prominence 0.293 and 22.7% prominent masks. Here, texture denotes images dominated by surface or material patterns, such as fabric, wood grain, asphalt, mesh, or repetitive façades.

## E Reference baseline detection method details

Figure 5 outlines the reference artifact-prominence baseline. The baseline first computes three heatmaps from existing quality and artifact-detection metrics, then fuses them with a lightweight MLP into a single prominence heatmap.

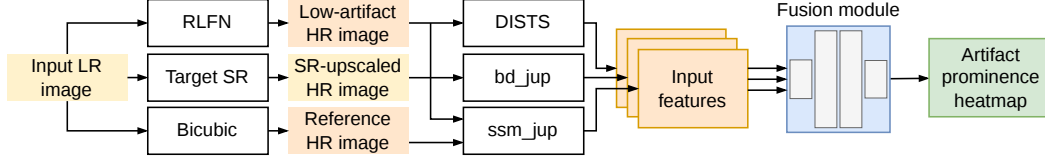


Figure 5: Architecture of the reference artifact-prominence baseline. The input image is upscaled by the target SR and compared against either the available HR reference or RLFN pseudo-GT as described in Section 5.3. Then, we compute three features described in Section E.1. Finally, we run the fusion module described in Section E.4.

## E.1 Input features

We selected features based on their proven performance for evaluating and detecting texture distortions. These features estimate not only the visual quality, but also the structural similarity between the reference and the upscaled image.

The first feature is DISTS [12], a visual-image-quality metric which accounts for texture distortions and their perceptual impact. As DISTS is trained on natural images, it effectively detects unnatural degradations like SR artifacts. DISTS produces a single image-level score, so we computed it block-wise in  $16 \times 16$ -pixel blocks, the minimum input size of the metric.

The second feature, which we call *ssm\_jup*, is adapted from the small-color-artifact detector from [23], itself based on LDL [3]. It targets small-scale distortions and was shown to be effective for finding JPEG AI artifacts. To capture texture distortions, we modify the detector to use all RGB channels rather than only chromatic U and V components. Like LDL, this feature requires a reference image upscaled by an artifact-resistant method; we chose bicubic interpolation for this input.

The last feature, *bd\_jup*, is a weighted sum of LPIPS [11] and ERQA [13] applied block-wise. LPIPS measures how well the upscaled image preserves perceptual quality, and is widely used in SR evaluation. Meanwhile, ERQA assesses the preservation of object details and boundaries. For LPIPS, we used  $32 \times 32$ -pixel blocks with stride of 16. ERQA uses  $8 \times 8$  blocks with no overlap. LPIPS is weighted 3:2 compared with ERQA.

We describe the implementation of the two custom features below.

## E.2 Structure Similarity Map (*ssm\_jup*)

Our *ssm\_jup* feature adapts the small-color-artifact detector from [23], which is itself based on LDL [3]. Given a reference image  $I_{\text{ref}}$  (the original HR or pseudo-GT), the SR output  $I_{\text{SR}}$ , and a bicubic-upscaled baseline  $I_{\text{bic}}$ , we compute scaled residual-variance maps for both SR and bicubic outputs.

First, we compute the absolute residual summed across channels:

$$R_x^C(i, j) = \sum_{c \in C} |I_x^c(i, j) - I_{\text{ref}}^c(i, j)|, \quad x \in \{\text{SR}, \text{bic}\}. \quad (1)$$

We then compute local variance within an  $n \times n$  window and scale it by a global factor:

$$M_x^C(i, j) = \text{var}\left(R_x^C\left(i - \frac{n-1}{2} : i + \frac{n-1}{2}, j - \frac{n-1}{2} : j + \frac{n-1}{2}\right)\right), \quad (2)$$

$$S_x^C(i, j) = \text{var}(R_x^C)^{1/5} \cdot M_x^C(i, j), \quad (3)$$

where  $n = 33$ .

The key modification from [23] is in the choice of color channels  $C$ : the original method computes separate maps on chrominance channels (UV from YUV and ab from Lab color spaces) and intersects the thresholded results to detect color artifacts. We instead operate on all three RGB channels ( $C = \{R, G, B\}$ ), which enables detection of luminance-correlated texture distortions that are common in SR artifacts but would be missed by chrominance-only analysis.

Table 8: Crowdsourced prominence across SR models on 6 datasets.

SR	Type	Masks Found	Mean Prominence	Conf. Masks Found
SeeSR	Diffusion	61	<b>7.15%</b>	0
ResShift	Diffusion	60	<u>7.20%</u>	0
SinSR	Diffusion	60	9.19%	2
HAT-L	Transformer	50	9.60%	1
DRCT	Transformer	50	13.33%	0
SwinIR	Transformer	60	17.12%	4
RealESRGAN	CNN	60	17.46%	5
SUPIR	Diffusion	62	17.56%	6

Table 9: Crowdsourced prominence across artifact detection methods on 6 datasets.

Method	Masks Found	Mean Prominence	Conf. Masks Found	Prom. × Conf.
ssm_jup (t=0.15)	80	7.42%	1	0.07
bd_jup (t=0.1)	80	7.34%	2	0.15
LDL (t=0.005)	80	9.46%	2	0.19
DeSRA	74	12.21%	3	0.37
<b>Baseline</b> (t=0.3)	70	<u>17.85%</u>	<b>8</b>	<b>1.43</b>
DISTS (t=0.25)	76	<b>18.03%</b>	<b>9</b>	<b>1.62</b>

The final feature is the smoothed difference between the SR and bicubic maps:

$$\text{ssm\_jup} = G_\sigma * S_{\text{SR}} - G_\sigma * S_{\text{bic}}, \quad (4)$$

where  $G_\sigma$  denotes a Gaussian kernel with  $\sigma = 33$ .

### E.3 Block-wise Distortion (bd\_jup)

The  $bd\_jup$  feature combines block-wise LPIPS [11] and ERQA [13] scores. LPIPS is computed on  $32 \times 32$  blocks with stride 16; ERQA uses  $8 \times 8$  blocks with no overlap. Since ERQA measures edge-preservation quality (higher is better), we invert it to obtain a distortion score. The final feature is:

$$\text{bd\_jup} = 0.6 \cdot \text{LPIPS} + 0.4 \cdot (1 - \text{ERQA}). \quad (5)$$

### E.4 Fusion module

We experimented with several architectures for fusing the features into a single prominence prediction, including CNN-based and tree-based models. A shallow multilayer perceptron (MLP) achieved the best overall performance, so we adopted it as our feature fusion module. The MLP takes as input the feature values, passes them through three fully connected layers (3-128-128-1) with ReLU activations, and outputs a single prominence value. It independently processes each pixel of the input-feature heatmaps, yet still captures broader context since the features themselves encode both the pixel’s neighborhood and wider image-level information.

### E.5 Training

We train our fusion module using Adam on a training subset of 374 artifact examples from Prominence-OpenImages. The model predicts a prominence value for each pixel of the input image. We compute the mean predicted prominence inside and outside the binary artifact mask from the dataset. The training loss consists of two  $L_2$  components:

$$\begin{aligned} \mathcal{L} = & L_2(\text{MeanInside}, \text{GT Prominence}) \\ & + L_2(\text{MeanOutside}, 0). \end{aligned} \quad (6)$$

The model is trained to predict the ground-truth prominence value inside the binary mask, and 0 (no artifact) outside it. Thanks to small model size, the training converges quickly, usually in around 10–15 epochs. One training epoch takes about 13 seconds on an Nvidia RTX 3090 GPU.

## F Subjective evaluation on additional SR datasets

We conduct an additional subjective evaluation on 6 widely known image datasets [33–37], following the setup described in Section 5.1. In total, this evaluation used 420 source images, each processed by 8 SR models.

Tables 8 and 9 show the results, grouped by SR models and by artifact detection methods, respectively. Interestingly, SR models show much better artifact robustness than in our main comparison in Section 6, likely because these datasets are commonly used for SR training and evaluation. Our baseline falls one confident artifact short of DISTS, but otherwise shows competitive results.

## G Artifact examples and failure cases

Figure 6 shows examples of prominent artifacts detected by our baseline across various SR models [1, 7, 2, 20, 24]. Each example is annotated with the binary artifact mask and subjective prominence.

Figure 7 shows examples of false detections by our baseline across SR models [32, 30, 29, 26]. We observed the following failure cases:

- Distortions on natural, unstructured objects, like ground, grass, or trees, that are not very prominent to human observers.
- Accurate restoration of fine textures such as fur, nylon, or mesh grille. False detections can happen on these when the lightweight SR (in our case, RLFN [22]) fails to produce a sharp upscaling of the texture, leading the metrics to see a discrepancy to the target SR and mark it as an artifact. Using an accurately-restored reference removes those false detections as Figure 8 shows.

Existing methods also suffer from these failure cases; indeed, they account for most of the low-prominence detections from our subjective evaluation described in Section 6.2.



Figure 6: Example artifacts detected by the baseline. (a): low-resolution input image; (b): target SR result with annotated output artifact mask; (c): artifact prominence heatmap predicted by our method; (d): our input features described in Sec. E.1, top to bottom: DISTs, bd\_jup, ssm\_jup.

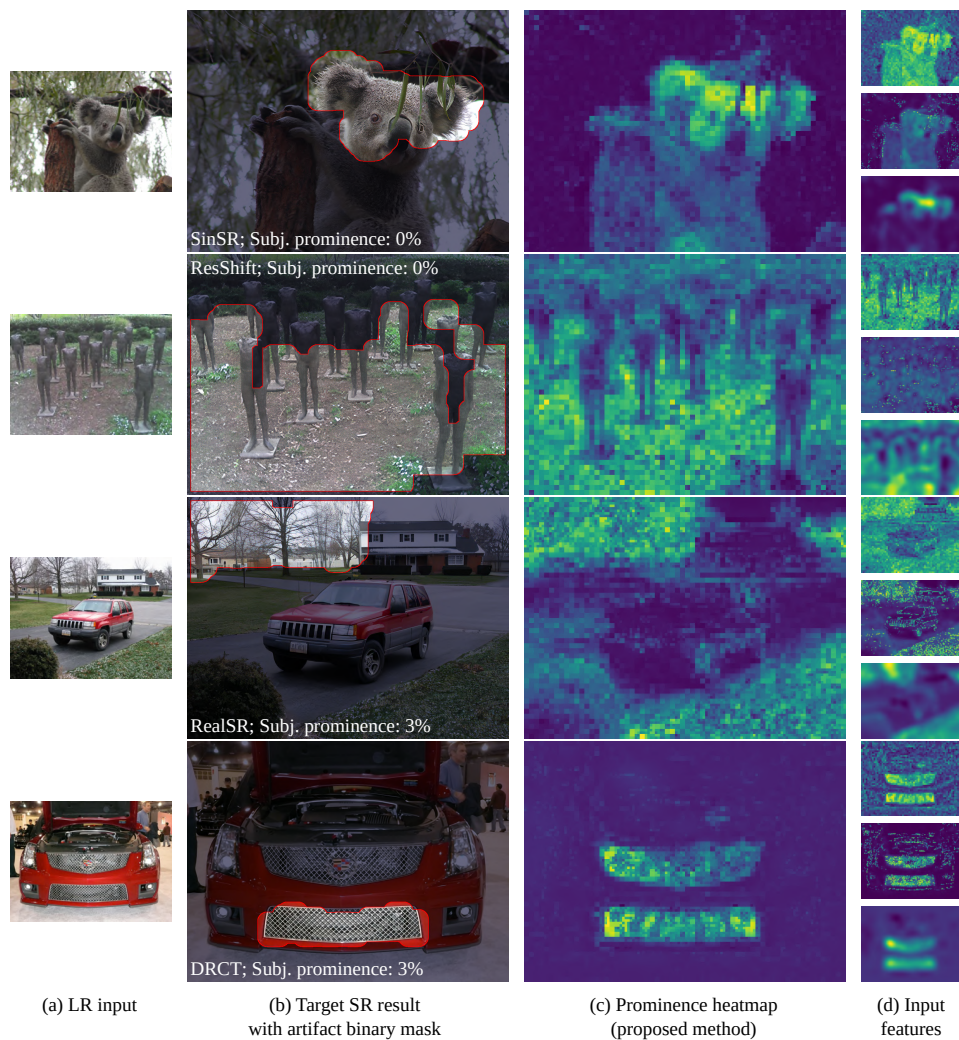


Figure 7: Example false detections by the baseline. (a): low-resolution input image; (b): target SR result with annotated output artifact mask; (c): artifact prominence heatmap predicted by our method; (d): our input features described in Sec. E.1, top to bottom: DISTS, bd\_jup, ssm\_jup.

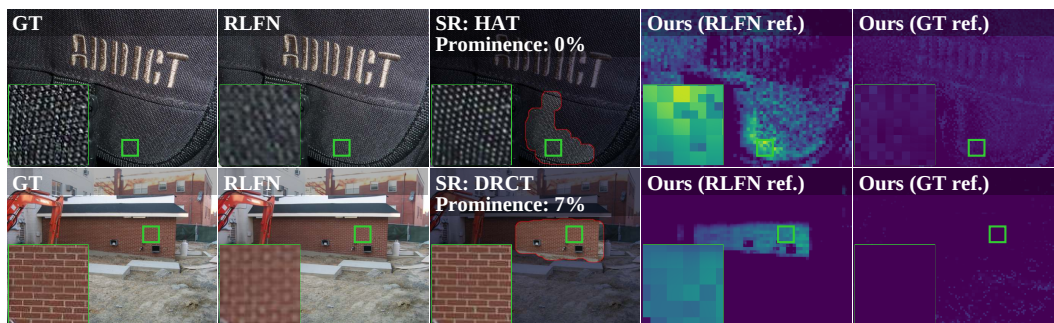


Figure 8: Example false detections by the baseline due to inaccurate restoration from pseudo-GT lightweight SR (RLFN). Rightmost column shows that the false detection disappears when an accurate restoration is used as reference instead of RLFN.